

RESEARCH ARTICLE

10.1002/2016PA002996

Key Points:

- This is the first study of mid-latitude Pliocene upwelling site warmth using a model that resolves the narrow upwelling front dynamics
- Effects of wind stress and ocean stratification, and of a newly proposed role for alongshore baroclinic pressure gradient, are quantified
- Even for dramatic changes in upwelling forcings, warming at proxy sites, >100 km from coast, is 3.4°, compared with 8° suggested by proxies

Correspondence to:

M. D. Miller,
madelinemiller@fas.harvard.edu

Citation:

Miller, M. D., and E. Tziperman (2017), The effect of changes in surface winds and ocean stratification on coastal upwelling and sea surface temperatures in the Pliocene, *Paleoceanography*, 32, 371–383, doi:10.1002/2016PA002996.

Received 30 JUN 2016

Accepted 27 MAR 2017

Accepted article online 4 APR 2017

Published online 18 APR 2017

The effect of changes in surface winds and ocean stratification on coastal upwelling and sea surface temperatures in the Pliocene

Madeline D. Miller¹  and Eli Tziperman^{1,2} 

¹Department of Earth and Planetary Sciences, Harvard University, Cambridge, Massachusetts, USA, ²School of Engineering and Applied Sciences, Harvard University, Cambridge, Massachusetts, USA

Abstract Sea surface temperature (SST) in subtropical eastern boundary upwelling zones is shown to be affected by three main factors: large-scale ocean stratification, upwelling-favorable sea surface wind stress, and the surface concentration (baroclinicity) of the alongshore pressure gradient driving the incoming geostrophic flow which balances the Ekman surface outflow. Pliocene-aged SST proxies suggest that some combination of differences in upwelling forcing enable the sea surface temperatures in these zones to increase by up to 11°C. We find that large warming in SST in response to the three factors, of up to about 10°C in addition to a mean Pliocene ocean warming of 2–3°C, is concentrated in the direct upwelling zone. In the location of proxy sea surface temperatures, about 120 km away from the coast, and outside the coastal upwelling zone, the SST response to changes in wind and stratification is weaker, only accounting for up to 3.4°C above the mean Pliocene warming. Increased baroclinicity of the alongshore pressure gradient has a smaller effect, accounting for less than 2°C increases at both the coast and proxy site. The SST seaward (westward) of the upwelling zone is primarily determined by ocean-atmosphere heat exchange and basin-scale ocean forcing, rather than by changes in upwelling. The spatial pattern of SST change with each of the three forcing factors is similar, and therefore, all could contribute to the Pliocene-modern difference in coastal SST.

1. Introduction

Proxy records show a 5–11°C sea surface warming at subtropical eastern boundary upwelling sites during the mid-Pliocene Warm Period (mPWP) relative to modern SSTs [Herbert and Schuffert, 1998; Marlow et al., 2000; Brierley et al., 2009; Dekens et al., 2007; Etourneau et al., 2009; LaRiviere et al., 2012; Fedorov et al., 2013]. Roughly 3°C of this temperature increase is consistent with the estimated global mean sea surface warming, but the balance requires further explanation. It has been proposed that the global ocean thermocline shoaled over the last 3 million years in response to global cooling, bringing cooler water within reach of the surface ocean upwelling [Philander and Fedorov, 2003; Boccaletti et al., 2004]. It has also been suggested that the thermocline may have shoaled over this time period due to the gradual closure of the Central American Seaway [Steph et al., 2010] or due to a reduction in tropical cyclones and subtropical ocean vertical mixing [Fedorov et al., 2010]. Another possibility is that upwelling-favorable surface winds were weaker due to the warmer global-scale SST and reduced sea-land temperature contrast during the mPWP [Arnold and Tziperman, 2015], an effect that is expected to reduce upwelling and its concomitant surface cooling. Thus, all previous hypotheses for the Pliocene mid-latitude upwelling site warmth involve either a change to the large-scale ocean stratification or to upwelling-favorable winds.

Coupled climate model simulations have been unable to reproduce the eastern boundary sea surface temperatures suggested by the proxies based on either of the two primary hypotheses [Dowsett et al., 2012; Haywood et al., 2013; Fedorov et al., 2013], despite the agreement that the paleoproxy data are high quality and predictive to at least ±2.5°C. Here we consider the hypothesis that missing or poorly parameterized physics, rather than data quality, is the cause of the data-model mismatch. A primary limitation of the coupled climate models is that the relatively coarse resolution of these models cannot capture the small-scale spatial variation in sea surface temperature at upwelling sites. Properly simulating SST at upwelling sites requires models of significantly higher resolution than is used for global climate studies, because the narrow coherent band of cool water due to upwelling is generally confined to within 10–50 km from the coast

[Small *et al.*, 2015; Renault *et al.*, 2012; Capet *et al.*, 2004; Enriquez and Friehe, 1995; Allen, 1980; Hurlburt and Thompson, 1973]. The modern SST in the direct upwelling zone/band can be 5° or more different from the modern SST at the offshore proxy sites and changes rapidly with distance from the shore [Marchesiello *et al.*, 2003; Marchesiello and Estrade, 2009; Capet *et al.*, 2008a]. Because the SST changes so dramatically within a few tens of kilometers, a model with grid scale of 10 km is required to capture the changes to the Pliocene upwelling dynamics, as done for the first time in this work.

There have been many studies of upwelling systems using idealized, sometimes analytic, models that illustrate the main factors participating in the upwelling dynamics [e.g., Pedlosky, 1978a, 1978b; Allen, 1973, 1980; Lentz and Chapman, 2004; Choboter *et al.*, 2005, 2011; Samelson and de Szoeke, 1988]. However, none of the analytic models have been able to represent the nonlinearities in a continuously-stratified configuration in a way that is fully consistent with observations. In addition, none of the idealized models attempted to capture the role of eddy heat and momentum fluxes which are now understood to be crucial in capturing the SST distribution. In a recent study, Spall and Schneider [2016] have been able to predict the offshore decay of an upwelling temperature perturbation using a simple model that included mixed-layer eddy effects but required the temperature at the coast to be known. This prevents the use of this theory as a predictive tool in the Pliocene context, where the temperature at the coast may vary significantly as a function of stratification, wind stress, and baroclinicity. Given these limitations of simple models and of coarse global general circulation models (GCMs), we choose in our study to use a high-resolution, eddy resolving, regional ocean model. This allows us to explore the roles of large-scale ocean stratification changes, wind stress, as well as of the alongshore baroclinic pressure gradient, a factor that has not been considered in the context of the Pliocene problem but is known to be important for coastal upwelling problems.

The Pliocene paleoproxy SST sites are all located over 100 km from the coast, so understanding the effect of upwelling on the changes between the Pliocene and modern requires understanding how the upwelling signal is transported westward/seaward along the surface. Modern observations and models find that eddies play an important role. They act to flatten the tilted isopycnals and transport heat toward the coast. The resulting cooling of the offshore waters carries the upwelling cooling signal away from the coast toward the proxy site. While submesoscale eddy fluxes dominate the vertical heat fluxes and participate in determining the mixed-layer depth, the mesoscale eddies responsible for the majority of the horizontal heat flux [Marchesiello *et al.*, 2003; Marchesiello and Estrade, 2009; Capet *et al.*, 2008a; Fox-Kemper *et al.*, 2008], and are therefore resolved in this study, unlike in previous GCM studies of the Pliocene upwelling problem.

Modern observations show that El Niño–Southern Oscillation generates anomalies of up to 4°C temperature and up to 5 m s⁻¹ (~0.03 N m⁻² using approximate conversion from Large and Pond [1982] and Trenberth *et al.* [1989]) in alongshore wind California Coastal System regional averages (time series unweighted average of six buoys between 35–39°N and 124–121°W [Schwing *et al.*, 2002]), but when spatial variability is considered, the typical anomalies are 1–2°C [Lynn and Bograd, 2002]. In modern observations, the local coastal anomalies are not distinguished from the Pacific basin average anomalies. Some of these effects may be due to stratification changes propagating from the tropics as coastally trapped Kelvin waves, and others can be due to atmospheric Rossby wave teleconnections affecting the wind. Modern observations also show a possible role for cloud feedbacks due to El Niño [Zaba and Rudnick, 2016], and these are not addressed here. Because the Pliocene record also shows a “permanent” El Niño [Wara *et al.*, 2005; Haywood *et al.*, 2007; Molnar and Cane, 2007; Scroxton *et al.*, 2011; Brierley *et al.*, 2009] or El Padre [Ravelo *et al.*, 2014; Ford *et al.*, 2015] state, these modern observations are relevant to our study, and we, indeed, explore the effects of both wind changes and stratification changes. The range of changes to these two forcing factors that we explore here are larger than those that can be attributed to El Niño, and additionally, the baseline mean El Padre state in the Pliocene would require another explanation for the higher-than-global average changes to SST in mid-latitudes.

Here we use an idealized configuration of a mesoscale-eddy-resolving regional ocean model to investigate how changes in surface wind stress, large-scale ocean stratification, and alongshore pressure gradient affect coastal upwelling and subsequently the SST in eastern boundary coastal upwelling zones. We find that the strong observed Pliocene changes in SST within the narrow upwelling zone adjacent to the boundary require what seem to be dramatic changes in these forcing factors and that the SST changes die off quickly with distance from the front position. Our results suggest that SST changes of the magnitude inferred from paleoproxies can only be expected inside the upwelling zone.

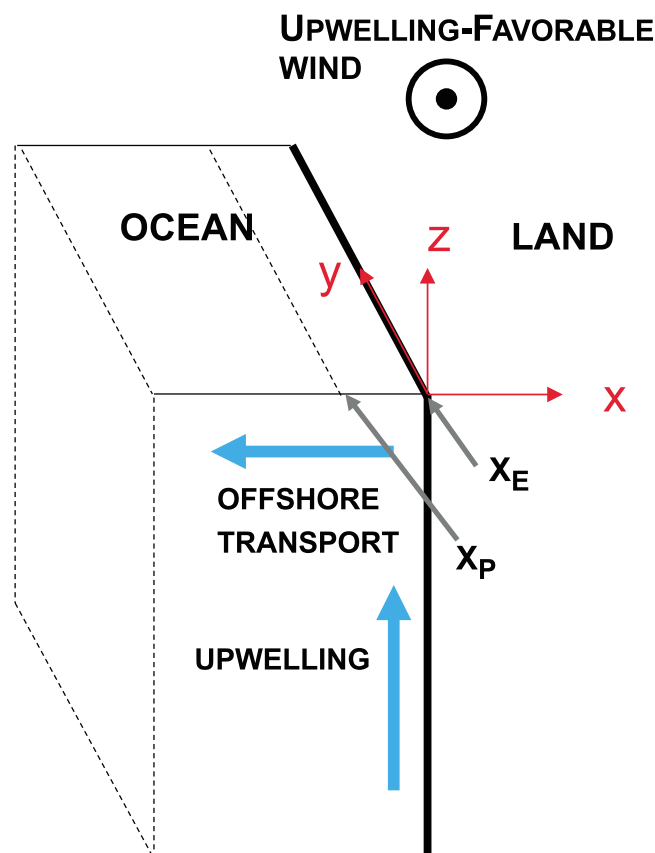


Figure 1. Domain schematic.

2. Ocean Model and Experiments

2.1. Model Configuration

We present a suite of numerical experiments from a regional ocean model of a mid-latitude coastal upwelling region. We use the Regional Oceanic Modeling System (ROMS) *Shchepetkin and McWilliams* [2003, 2005], specifically the ROMS-AGRIF version [Debreu *et al.*, 2012; Penven *et al.*, 2006]. Our test case is modeled after the Southern California proxy location (Ocean Drilling Program site 1014, 32°50'N, 119°59'W). The domain is flat bottomed, centered at 33°N, and dimensioned 560 km × 560 km by 1500 m deep, based on Cartesian coordinates (x, y) corresponding to (east, north) as shown in Figure 1. We do not include coastal bathymetry because we cannot resolve the rapid dropoff of the continental shelf, and our choice is supported by the work of Capet *et al.* [2008a, 2008b, 2008c] that find good agreement between simulation and observations despite the lack of shelf bathymetry. The vertical discretization is 35 sigma levels. We use the default "Transformation 2" ($V_{transform} = 2$ and $V_{stretching} = 4$) as detailed in the ROMS documentation

(https://www.myroms.org/wiki/Vertical_S-coordinate) with $\Theta_s = 4$ (stretching coordinate for the surface boundary layer), $\Theta_b = 0$ (no stretching in the bottom boundary layer) and $H_c = 200$ m.

Modern observations of coastal boundary upwelling sites find a significant alongshore pressure gradient and that the offshore surface Ekman transport is approximately balanced by a broad (in z) geostrophic onshore inflow driven by the pressure gradient [Lentz and Chapman, 2004]. The pressure gradient during the Pliocene is not known, of course, and we therefore treat it as one of our model parameters. For this purpose, we show results from an f -plane configuration, with meridionally periodic boundary conditions and with a body force added to the momentum equations that is equivalent to $\partial P / \partial y$. Without the body force or a meridional pressure gradient, the onshore and offshore flows (in the x direction) are unrealistically confined to surface and bottom Ekman layers, and the use of periodic boundary conditions allows us to add the meridional pressure gradient as needed. In our Control experiment, the body force is barotropic (constant in z) and is constructed to exactly balance the offshore Ekman mass transport driven by the surface wind forcing. The body force is constant in y and t but is a function of x (offshore position) as dictated by the x variations of the surface wind stress. Our sensitivity experiments explore the effect of different vertical structures of the meridional pressure gradient on the SST.

We include frictional dissipation due to bottom linear drag, $-ru$, with $r = 5 \times 10^{-4} \text{ m s}^{-1}$. There is a wall at the eastern boundary representing the coast, where we prescribe a free-slip boundary condition on the meridional velocity, zero zonal velocity, and a zero gradient for tracers. At the western boundary we use nudging toward the initial vertical temperature profile, and a radiation boundary condition for the velocities. The horizontal tracer advection scheme is TS_HADV_RSUP3 which reduces spurious diapycnal mixing in terrain-following coordinate models [Marchesiello *et al.*, 2009], and we represent subgridscale vertical mixing with the K-Profile Parameterization [Large *et al.*, 1994].

The surface wind stress is uniform in y and varies in x from 0 N m^{-2} at the coast to an offshore maximum at -40 km (motivated by observations [e.g., Capet *et al.*, 2004; Edwards *et al.*, 2001; Renault *et al.*, 2012]),

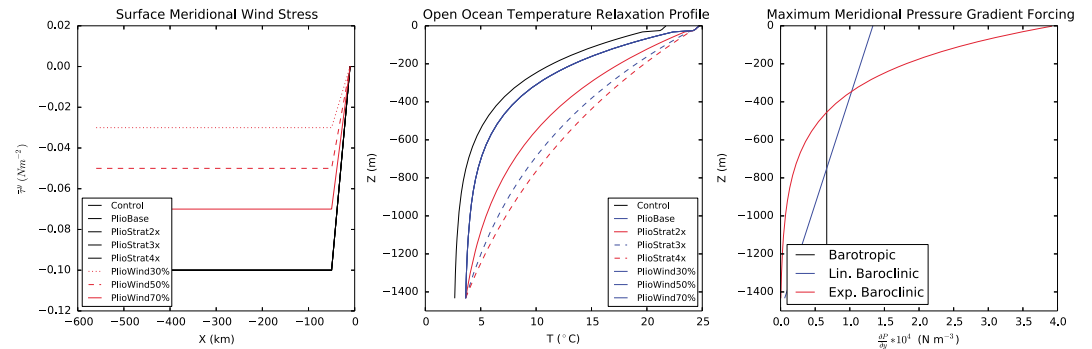


Figure 2. Surface wind forcing, prescribed offshore restoring temperature profile $\bar{T}^{y,t}(z)$ and the vertical structure of the prescribed meridional (N-S) pressure gradient for all experiments. The exponential fit in the offshore restoring temperature profile begins at the base of the mixed layer, as determined by the depth in the WOA summer decadal average data set at which the temperature difference from the surface is less than 0.5°C .

remaining constant further offshore (Figure 2). The initial conditions are a horizontally uniform temperature profile (Figure 2) based in the control case on the World Ocean Atlas 2013 $\frac{1}{4}^\circ$ multidecadal average summer vertical temperature profile at 33°N and 140°W [WOA13 [Locarnini *et al.*, 2013]]. Salinity is constant and homogeneous in these experiments, and the velocities are initialized to zero everywhere.

We relax the temperature at the sea surface to the SST in the temperature profile used for initial conditions using an air-sea heat flux calculated as

$$\rho_0 C_p \frac{dT}{dt} \sim Q_{\text{model}} = Q^* - \Gamma(T - T_{\text{relax}}) \quad (1)$$

where T_{relax} is the sea surface temperature in the restoring profile, Q^* is a constant background heat flux equal to -50 W m^{-2} appropriate for the ocean at this latitude losing heat on a global average (note that this would have a positive sign in the traditional definition of upward ocean heat flux), and $\Gamma = 30 \text{ W m}^{-2} \text{ K}^{-1}$ similar to measurements at this latitude [Gill, 1982; Haney, 1971].

2.2. Experiments

We run each experiment for 20 model years. The experiments all reached a statistical steady state in less than 2 years, based on time series of domain-average horizontal kinetic energy, available potential energy, and horizontal enstrophy. We take averages over the final 10 years of each experiment. The Control experiment is modeled after modern upwelling-favorable (summer) conditions in Southern CA and has a maximum southward surface wind stress of 0.1 N m^{-2} [e.g., Pickett and Paduan, 2003]. Our specified offshore (western boundary) temperature profile is obtained by fitting an exponential profile to the WOA13 temperature data at 33°N , 140°W of the form

$$T(z) = a e^{z/H_0} + b, \quad (2)$$

finding $a = 21.2$, $b = 3.67$, $H_0 = 257.75$ (black curve in Figure 2). The restoring temperature profile for the base Pliocene case (PlioBase, Table A1) is obtained from the Control profile by varying a , b to warm the surface and bottom temperatures by $\Delta T_s = 3^\circ\text{C}$ and $\Delta T_b = 2^\circ\text{C}$, respectively. Pliocene bottom water temperature estimates are sparse, and the maximum 10% of existing anomaly (calculated as Pliocene-Modern) estimates range from -1.9 to 4.2°C , with most of the anomalies less than 1.0°C [Dowsett *et al.*, 2009]. Therefore, 2.0°C is a conservatively (perhaps excessively) large value for the Pliocene deep ocean. The largest annual mean surface atmospheric temperature anomaly in the Pliocene simulated by coupled climate models is 3°C average, and the simulated annual mean global SST anomalies are $\sim 2^\circ\text{C}$, though there is significant spatial variability in estimated and simulated Pliocene SST [Dowsett *et al.*, 2012; Fedorov *et al.*, 2013; Haywood *et al.*, 2013].

We examine the upwelling response to both stratification and wind using two sets of experiments termed PlioWind and PlioStrat. The PlioWind experiments have the same temperature forcing profile as the PlioBase

experiment and vary only in the maximum surface wind stress (e.g., PlioWind50% has a maximum wind stress equal to 50% of that of the Control). The PlioStrat experiments have the same surface wind stress as the Control, surface and bottom water shifts equivalent to those in PlioBase, and vary only in their decay scale H , representing different degrees of vertical stratification. The values used for each experiment are tabulated in Table A1.

The surface enhancement, or baroclinicity, of the meridional pressure gradient controls the depth from which water upwells. To demonstrate the sensitivity of the SST to variations in the deep alongshore pressure gradient, we present two experiments in which we vary the baroclinicity of the meridional pressure gradient. In both, the pressure gradient has a maximum at the sea surface and decays with depth to zero at the bottom of the domain. In the “Linear Baroclinic” experiment, the decay is a linear function of depth, while in “Exponential Baroclinic” the decay is exponential with depth (Figure 2).

3. Results

Reductions in the upwelling-favorable wind stress or the temperature stratification (prescribing a deeper thermocline via a larger exponential scale H in equation (2)) both lead to an increase in the meridionally-averaged and time-averaged SST ($\overline{SST}^{y,t}$) relative to Control (Figure 3 and Table A1). The $\overline{SST}^{y,t}$ also increases with increasing baroclinicity (surface concentration) of the meridional pressure gradient because this baroclinicity causes the inflow to occur at shallower depths and the upwelling water is therefore warmer (Figure 4 and Table A1). In all cases, excluding PlioBase which we explain below, the $\overline{SST}^{y,t}$ response to the forcing changes is greatest closest to the coast and decays monotonically with distance from the coast to an almost constant value. For simplicity we focus our discussion of the results on two specific surface locations: the eastern boundary, x_E , and a site 120 km offshore, representing a typical proxy location, x_p . We tabulate the numerical results in Table A1 in Appendix A, where we also provide a linear fit to the coastal warming at the two locations as function of the stratification and wind changes.

The change in forcing in PlioBase with respect to Control is a constant 2°C shift in the temperature forcing profile and a further increase in vertical temperature stratification via an increase in surface-deep temperature difference of 1°C (section 2.2). At x_E , the resulting steady-state $\overline{SST}^{y,t}$ increase (relative to Control) is 2.3°C, close to the prescribed 2°C shift in the restoring profile’s bottom water temperature. In contrast, $\Delta\overline{SST}^{y,t}$ at x_p is 2.9°C, 0.1°C less than the prescribed restoring profile’s surface temperature shift of 3°C. This result, in addition to the fact that most of the temperature restoring profile is simply shifted by a constant 2°C (Figure 3, the change in stratification between Control and PlioBase is confined to the upper levels), suggests that water is upwelling from the same depth in Control and PlioBase. Conversely, similarity between $\overline{SST}^{y,t}$ at x_p and the surface relaxation temperature indicate that the large-scale ocean forcing and atmosphere-ocean heat flux are the dominant controls on $\overline{SST}^{y,t}$ at x_p .

Experiment PlioExtreme, which simulates a dramatic scenario of a 30% reduction in wind and a doubling of the stratification depth scale, shows a further increase in $\overline{SST}^{y,t}$ relative to PlioBase of 4.6°C at x_E and 2.7°C at x_p , still insufficient to explain the Pliocene observations. A linear summation of the responses to forcing changes in PlioWind70% and PlioStrat2x would predict an increase from PlioBase to PlioExtreme in $\overline{SST}^{y,t}$ of 5.0°C at x_E and of 2.8°C at x_p . The increase in $\overline{SST}^{y,t}$ from PlioBase to PlioExtreme is damped relative to the prediction from the linear combination of forcing shifts of PlioStrat2x and PlioWind70%: 92% of the linear combination at x_E and 96% of the linear combination at x_p .

The structure of the temperature and velocity fields is similar in the Control and PlioExtreme experiments; however, the offshore mass transport and the deep inflow of cold water is reduced in PlioExtreme, leading to overall warmer surface temperatures (Figure 5). The depth at which the u velocity changes sign is approximately –20 m in both cases. The offshore velocity in the upper 10 m is reduced in PlioExtreme, consistent with the reduced surface wind forcing.

The steady-state mixed-layer temperature budget (Figure 6) shows that $\overline{SST}^{y,t}$ is set by a balance between upwelling (vertical advection of heat from below, $\sim wT$), offshore transport (x advection), and surface forcing, in this case the air-sea heat flux (equation (1)). The x advection and vertical advection are the largest

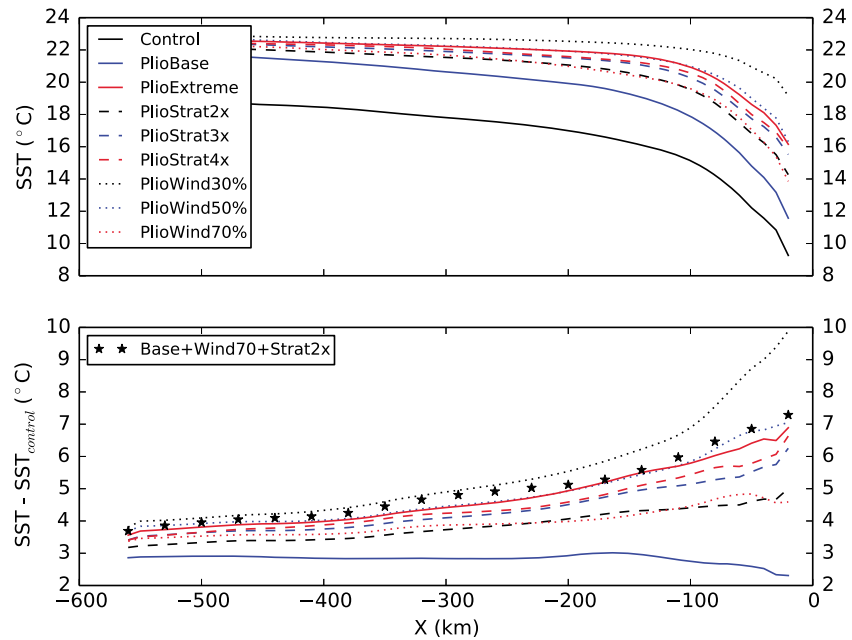


Figure 3. (top) Time- and y-mean SST ($\overline{SST}^{y,t}$) from all experiments. (bottom) Difference in $\overline{SST}^{y,t}$ between Plio-experiments and Control.

components of the steady state budget. The main difference between Control and PlioExtreme temperature budgets is that the surface forcing is reduced, as the water upwelled is warmer (closer to the relaxation temperature).

The onshore temperature advection (x advection) can be decomposed into a mean (time and y) component $\frac{\partial}{\partial x}(\overline{uT}^{y,t})$ and an eddy component $\frac{\partial}{\partial x}(\overline{u'T'}^{y,t})$, where $u = \overline{u}^{y,t} + u'$. While the total onshore x advection of temperature is similar in both the Control and PlioExtreme cases (Figure 6), the eddy component is reduced

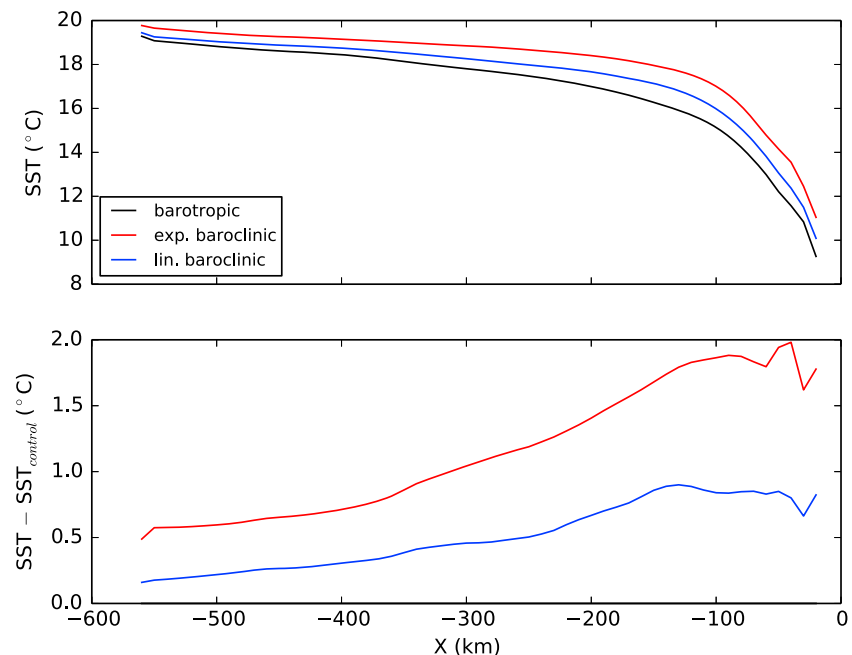


Figure 4. (top) Time- and y-mean SST ($\overline{SST}^{y,t}$) from Control (barotropic), Linear Baroclinic, and Exponential Baroclinic experiments. (bottom) Difference in $\overline{SST}^{y,t}$ between baroclinic experiments and barotropic Control.

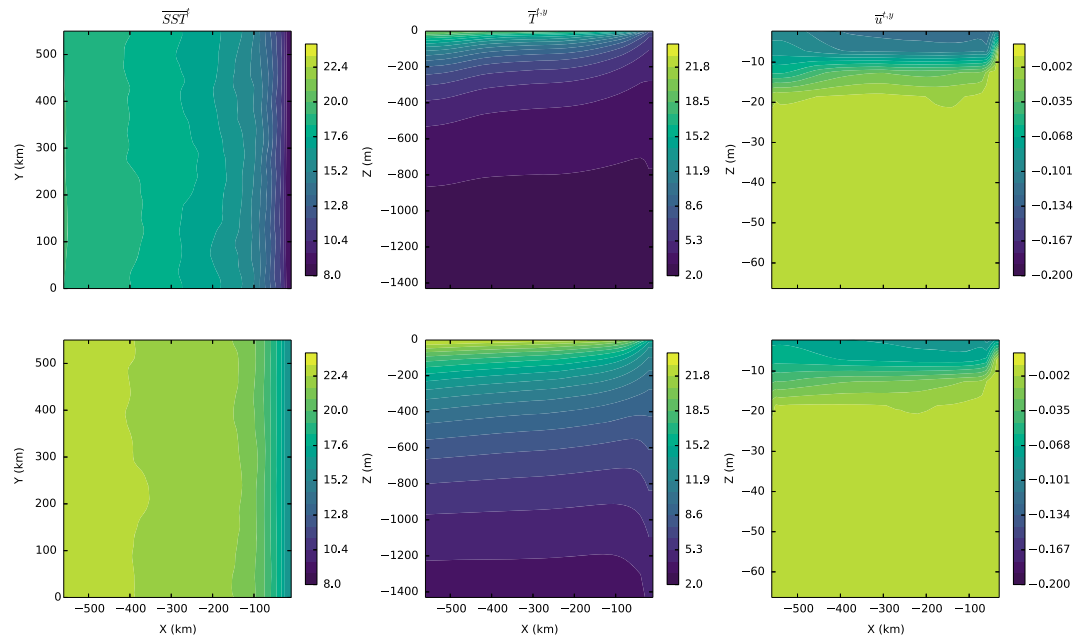


Figure 5. Time-mean SST and time- and y-mean temperature and u velocity for Control and PlioExtreme experiments.

in the PlioExtreme case (not shown). The surface eddy strength and variability is similar in the velocity fields, but the eddy strength and variability of the SST field is decreased in the PlioExtreme case, because there is a smaller horizontal temperature gradient for the eddies to feed on and advect (Figure 7).

Recent work suggests that the position and strength of upwelling fronts, and ocean fronts in general, is strongly influenced by submesoscale eddies and their effect on the mixed-layer depth, which cannot be represented by a 10 km resolution ocean [Fox-Kemper *et al.*, 2008; Fox-Kemper and Ferrari, 2008]. However, even when the submesoscale eddies are resolved, the horizontal heat transport (which determines the value of SST

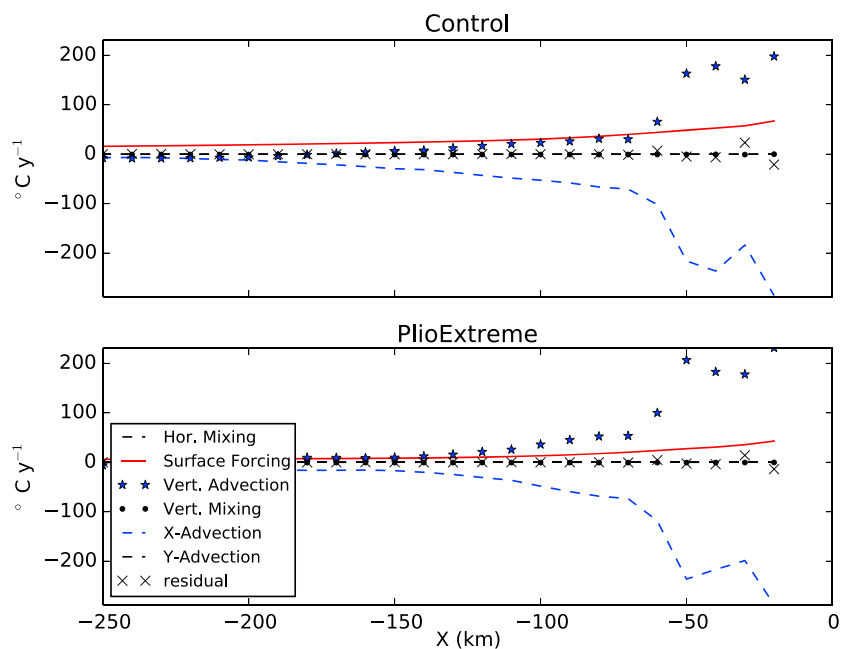


Figure 6. Steady state mixed-layer (32 m) temperature budget for (top) Control and (bottom) PlioExtreme.

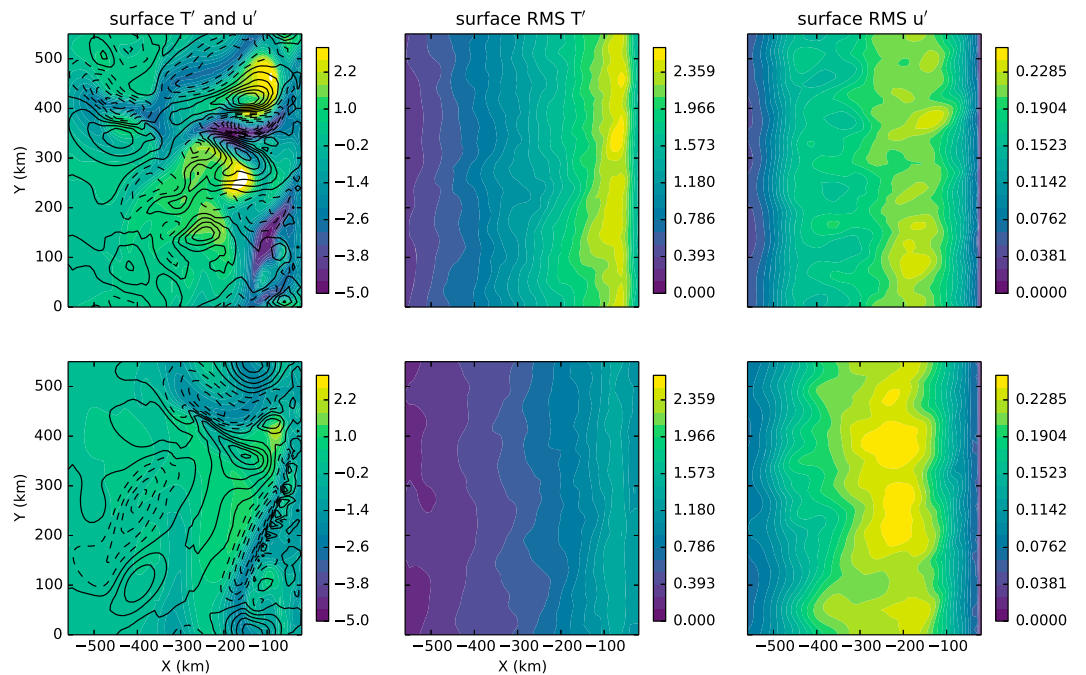


Figure 7. Snapshot of T' (colors) and u' (lines), root-mean-square (RMS) surface T' , and root-mean-square (RMS) u' for (top row) Control and (bottom row) PlioExtreme. Snapshot u' levels are 0.103 m/s, negative values are dashed lines, and positive values are solid lines. The time sampling interval for eddy values is 5 days.

at the proxy site) is dominated by the mesoscale eddy heat transport which act to flatten isopycnals and flux heat toward the coast [Capet et al., 2008a]. Still, the depth of the mixed layer, which would affect the depth from which water upwells, is sensitive to submesoscale vertical eddy heat transport.

Spall and Schneider [2016] developed a one-dimensional steady-state analytical model and scaling for the offshore decay of a negative upwelling perturbation in $\overline{SST}^{y,t}$ with distance from the coast, showing that for the simplest case they consider, the decay scale is given by $L = \frac{\tau_0 C_p}{f_0 \Gamma}$, in terms of the wind stress magnitude τ_0 , Coriolis parameter f_0 , specific heat of water C_p , and the atmospheric-ocean heat exchange sensitivity to temperature difference Γ . In our experiments this scale is 120–170 km, explaining why the effect of changes in coastal upwelling at the proxy site is significantly weaker than at the coast. It is important to note that this analytical theory requires that the temperature at the coast, T_{\min} is known. Therefore, this theory is not predictive of the SST distribution given an arbitrary ocean stratification, wind forcing, and meridional pressure gradient. Additional details and figures comparing the Spall and Schneider [2016] theory and our numerical simulations are shown in Appendix B.

4. Discussion and Conclusions

In our experiments, the $\overline{SST}^{y,t}$ inside the upwelling zone is much more sensitive to changes to the three upwelling forcing factors considered here than the $\overline{SST}^{y,t}$ at the proxy site. The changes in $\overline{SST}^{y,t}$ within the upwelling zone due to altered wind, stratification, and large-scale baroclinicity could combine to create $\overline{SST}^{y,t}$ anomalies equal in magnitude to the reported Pliocene-Modern difference in coastal boundary $\overline{SST}^{y,t}$. Temperature anomalies up to 8°C above the global mean implied by proxies could reasonably have been due to changes in upwelling, if the proxy measurements were inside the upwelling zone (although the necessary changes in forcing factors are very large and not simply explained). However, all of the relevant proxy locations are over 100 km from the coastal boundary, far outside the modern upwelling zone, and the mean horizontal temperature transport from the upwelling zone to the proxy site is a minor component of the temperature budget at that point. Instead, much of the change in $\overline{SST}^{y,t}$ between the Control and Plio-experiments at the

proxy site can be explained by the base shift of 3°C in the SST forcing, with no more than 3.4°C additional change due to even an extreme reduction of upwelling-favorable winds.

High biogenic sedimentation occurs when/where nutrients are available and is therefore enhanced where cold upwelling water is found. That implies that the proxies may record colder temperatures than the mean. The larger eddy variability found in our modern simulation would lead to a stronger RMS of the SST away from the coast (Figure 7 (top row, middle)) and therefore a possibly larger colder bias than in the Pliocene that has a smaller RMS (Figure 7 (bottom row, middle)). This may explain part of the cooling seen in the record, yet the difference in RMS between the two runs at 100 km away from the coast is only about 1°C, significant yet too small to account for the observed difference between the present-day and Pliocene temperatures.

One additional factor that may affect the large change in SST at the proxy site is that the width of the coastal upwelling zone may have expanded between the Pliocene and Modern, putting the proxy site closer to the present-day upwelling zone. The modern upwelling zone width is 10–30 and at maximum 50 km wide [Pickett and Paduan, 2003; Edwards et al., 2001; Marchesiello and Estrade, 2010]. This width of the upwelling zone is sensitive to the absolute magnitude of the wind stress [Capet et al., 2004; O'Brien and Hurlburt, 1973], and because the Pliocene upwelling-favorable wind stress is expected to have been somewhat reduced [Arnold and Tziperman, 2015], the upwelling zone may have expanded since the Pliocene. This would lead to some cooling offshore, but given our results and the decay scale predicted by Spall and Schneider [2016], the effect is expected to be small at 100 km from the coast.

There are further challenges in directly comparing modern observed SST to proxy SST in coastal upwelling zones caused by the sparsity of modern observations, the temporal and spatial variability of both upwelling and SST and the variability of the proxy dependence on temperature (some proxies reflect annual averages while some reflect seasonal averages or seasonal maxima). In a study of the Canary Current upwelling off Cape Ghir, for example, McGregor et al. [2007] notes the variability in different choices of “modern” SST at their study site is approximately 3°C.

Strong coupling between atmospheric temperature, wind stress, and SST has been observed in upwelling zones, and the coupling further affects both the latent and sensible heat fluxes that determine the thermocline depth [Chelton et al., 2004, 2007]. We ignore this complex air-sea interaction by using a constant relaxation surface temperature. Additionally, in some upwelling regions, upwelling is intermittent or seasonal, while in others the upwelling conditions persist throughout the year. The cases we considered reflect a persistent upwelling case. Intermittent wind forcing and upwelling, a process not represented in this study, would tend to weaken the cooling effect of upwelling on SST, causing the time-average SST values to be closer to the large-scale temperature forcing profile.

The model experiments here are able to resolve upwelling zone dynamics for the first time and to explore the role of three main forcing factors on the SST in upwelling zones. We conclude that the Pliocene warming of upwelling zones remains a mystery: our results cannot explain a large-amplitude observed warming at a distance of some 100 km from the coast even if we allow for significant changes to the wind, stratification and the baroclinicity of the alongshore pressure gradient.

Appendix A: Parameters and Table of Results

Table A1 summarizes the parameters varied in the model experiments and the steady-state meridional average response, $\overline{SST}^{y,t}$, at the coast and the proxy site. The change in $\overline{SST}^{y,t}$ at the coast and at the paleoproxy measurement site with respect to PlioBase can be approximately expressed by a linear fit. We define the quality of fit as

$$\frac{\sum_{i,j} |\Delta_{\text{plio}} \text{SST}|_{\text{model}}(H_i, \tau_j) - \Delta_{\text{plio}} \text{SST}|_{\text{fit}}(H_i, \tau_j)|^2}{\sum_{i,j} |\Delta_{\text{plio}} \text{SST}|_{\text{model}}(H_i, \tau_j)|^2} \quad (\text{A1})$$

where the sum is over the values of stratification and wind stress that have been used in the model runs. The fits are given by $\Delta_{\text{plio}} \text{SST}|_{x_g} \approx 100(\tau - \tau_{\text{ctrl}}) + 6.5 \times 10^{-3}(H - H_0)$ (quality is 0.14) and $\Delta_{\text{plio}} \text{SST}|_{x_p} \approx 50(\tau - \tau_{\text{ctrl}}) + 3.5 \times 10^{-3}(H - H_0)$ (quality is 0.13). The units of the linear fit coefficients ΔSST , H , and τ are respectively °C, m, and N m^{-2} .

Table A1. Parameters Used in Model Experiments, Describing the Degree to Which the Stratification and Wind Stress Are Varied in Each, and Summary of Changes in SST at the Coast and Proxy Site in Each Experiment^a

Experiment	τ_{\max}	ΔT_s	ΔT_b	H	$\Delta \text{SST} _{x_E}$	$\Delta_{\text{plio}} \text{SST} _{x_E}$	$\Delta \text{SST} _{x_p}$	$\Delta_{\text{plio}} \text{SST} _{x_p}$
Control	-0.1	0	0	H_0	-	-	-	-
Lin. Baroclinic	-0.1	0	0	H_0	0.8	-	0.9	-
Exp. Baroclinic	-0.1	0	0	H_0	1.8	-	1.8	-
PlioBase	-0.1	3	2	H_0	2.3	-	2.9	-
PlioExtreme	-0.07	3	2	$2H_0$	6.9	4.6	5.6	2.7
PlioWind70%	-0.07	3	2	H_0	4.6	2.3	4.3	1.4
PlioWind50%	-0.05	3	2	H_0	7.1	4.7	5.5	2.6
PlioWind30%	-0.03	3	2	H_0	9.9	7.6	6.4	3.4
PlioStrat2x	-0.1	3	2	$2H_0$	5.0	2.7	4.3	1.4
PlioStrat3x	-0.1	3	2	$3H_0$	6.3	3.9	5.0	2.1
PlioStrat4x	-0.1	3	2	$4H_0$	6.6	4.3	5.2	2.3
Wind70% + Strat2x						5.0		2.8

^a H (m) is the exponential decay scale of the prescribed temperature profile, $H_0 = 257.75$ m is calculated from present-day observations for the control run, τ_{\max} (N m^{-2}) is the maximum wind stress, and $\Delta T_{s,b}$ ($^{\circ}\text{C}$) are the specified warming of the surface and bottom restoring temperature profile relative to the control case. ΔSST ($^{\circ}\text{C}$) is the difference between the sensitivity and Control experiment and $\Delta_{\text{plio}} \text{SST}$ is the difference between sensitivity and PlioBase experiment. x_E denotes the position of the eastern boundary of the domain and x_p is the position of the paleoproxy measurement, 120 km from the coast.

Appendix B: Comparison to Spall and Schneider [2016]

Spall and Schneider [2016] developed a one-dimensional steady-state analytical model and scaling for the offshore decay of a negative upwelling perturbation in SST with distance from the coast, $T(x) - T_{\min}$, where x is transverse distance from the coast and T_{\min} is the SST at the coast, which must be specified. T_{\min} in Spall and Schneider [2016] is equivalent to the coastal temperature that we call x_E . The decay scale is a function of the wind stress magnitude τ_0 , Coriolis parameter f_0 , specific heat of water C_p , and the atmospheric-ocean heat exchange sensitivity to temperature difference Γ ,

$$L = \frac{\tau_0 C_p}{f_0 \Gamma} \tag{B1}$$

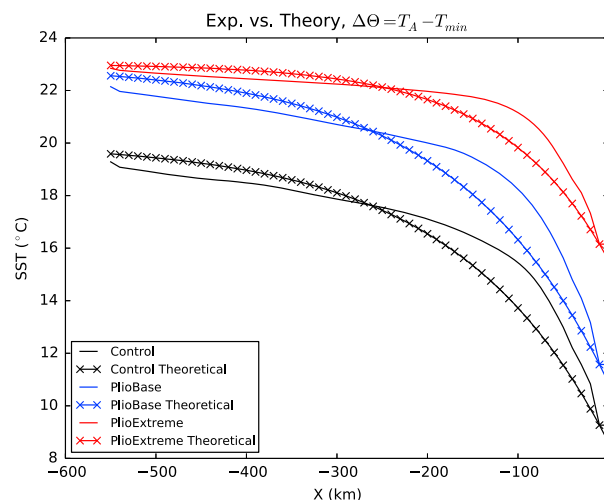


Figure B1. $\overline{\text{SST}}^{y,t}$ from Control, PlioBase, and PlioExtreme experiments compared to theoretical $\overline{\text{SST}}^{y,t}$ predicted by Spall and Schneider [2016] without mixed-layer eddy parameterization.

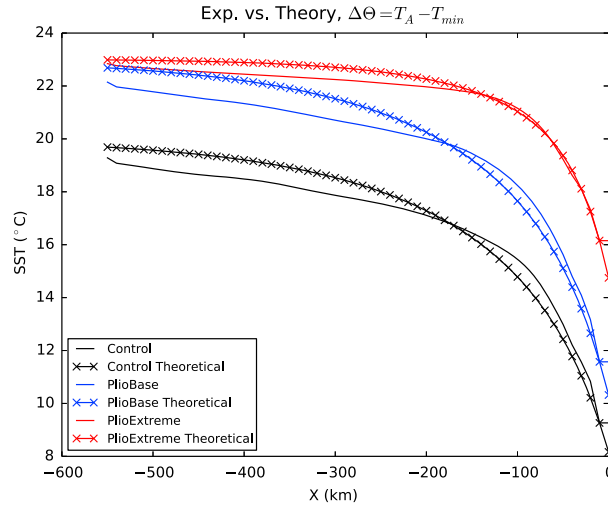


Figure B2. $\overline{SST}^{y,t}$ from Control, PlioBase, and PlioExtreme experiments compared to theoretical $\overline{SST}^{y,t}$ predicted by *Spall and Schneider* [2016] including mixed-layer eddy parameterization.

Our Control experiment parameters predict that $L \sim 170$ km and our PlioExtreme experiment parameters predict that L is ~ 120 km. In the case of a fixed atmospheric temperature and no ocean eddies,

$$T_{\text{pred}}(x) = T_{\text{min}} + \left(\Delta\Theta + \frac{Q^*}{\Gamma} \right) (1 - e^{\hat{x}}) \quad (\text{B2})$$

where $\Delta\Theta = T_{\text{relax}} - T_{\text{min}}$ and $\hat{x} = \frac{x}{L}$ and where we take the sign convention of x to be negative offshore (see Figure 1) and Q^* and Γ have the same definition and values as in equation (1). In the absence of a background heat flux, the offshore temperature would reach 60% of the atmospheric relaxation temperature within the decay scale L . The background heat flux alters the maximum offshore temperature, but the decay scale of the cold upwelling perturbation remains the same.

Plotting our steady state meridional average $\overline{SST}^{y,t}$ in comparison to that predicted by *Spall and Schneider* [2016] in Figure B1 we see that their basic theory (crosses) predicts a smoother and broader decay than our numerical results (lines).

Spall and Schneider [2016] then include also the parameterized effect of mixed-layer eddies, relying on *Fox-Kemper et al.* [2008], and then predict

$$T = \mu \left(-Q^2 A_2^2 + Q A_2^3 - \frac{1}{3} A_2^4 + \frac{1}{3} A_2^4 - Q A_2^3 + Q^2 A_2^2 \right) \quad (\text{B3})$$

where $A_2 = 1 + \frac{Q^*}{\Gamma \Delta\Theta}$ and $Q = \frac{Q^*}{\Gamma \Delta\Theta}$ and $\mu = \frac{c_e g \alpha_0 \Gamma \Delta\Theta^3 f_0}{c_p \tau_0^2 T_z^2}$. $c_e = 0.015$ is an empirical constant, α_0 is the thermal expansion coefficient of the water, here chosen to be a constant $0.2 \text{ kg m}^{-3} \text{ K}^{-1}$. T_z is the vertical derivative of the background ocean temperature stratification, right below the mixed layer (in the thermocline) and which is 0.07 K m^{-1} in our control and PlioBase experiments, and 0.04 K m^{-1} in PlioExtreme (Figure B2).

It is important to note that while the analytical theory when mixed-layer eddies are included is a good predictor of the temperature distribution as a function of distance from the coast (Figure B2), it requires that the temperature at the coast, T_{min} is known. Therefore, it explains why the temperature at the coast is different from the temperature at the paleoproxy site, but it is not predictive of the SST distribution given an arbitrary ocean stratification, wind forcing, and meridional pressure gradient (which may or may not be baroclinic).

References

- Allen, J. S. (1973), Upwelling and coastal jets in a continuously stratified ocean, *J. Phys. Oceanogr.*, *3*, 245–257.
- Allen, J. S. (1980), Models of wind-driven currents on the continental shelf, *Annu. Rev. Fluid Mech.*, *12*, 389–433.
- Arnold, N. P., and E. Tziperman (2015), Reductions in midlatitude upwelling-favorable winds implied by weaker large-scale Pliocene SST gradients, *Paleoceanography*, *31*, 27–39, doi:10.1002/2015PA002806.
- Boccaletti, G., R. C. Pacanowski, S. G. H. Philander, and A. V. Fedorov (2004), The thermal structure of the upper ocean, *J. Phys. Oceanogr.*, *34*, 888–902, doi:10.1175/1520-0485(2004)034.

Acknowledgments

This work was supported by NASA grant NNX14AH39G and by the NSF Physical Oceanography program, grant OCE-1535800. Computational resources were provided by the NASA High-End Computing (HEC) Program through the NASA Center for Climate Simulation (NCCS) at Goddard Space Flight Center. Both M.D.M. and E.T. thank the Weizmann Institute of Science for its hospitality during parts of this work. ROMS input files for the experiments in the manuscript are available by emailing the corresponding author M.D.M. (madelinemiller@fas.harvard.edu).

- Brierley, C. M., A. V. Fedorov, Z. Liu, T. D. Herbert, K. T. Lawrence, and J. P. LaRiviere (2009), Greatly expanded tropical warm pool and weakened Hadley circulation in the early Pliocene, *Science*, *323*, 1714–1718, doi:10.1126/science.1167625.
- Capet, X., P. Marchesiello, and J. C. McWilliams (2004), Upwelling response to coastal wind profiles, *Geophys. Res. Lett.*, *31*, L13311, doi:10.1029/2004GL020123.
- Capet, X., J. C. McWilliams, M. J. Molemaker, and A. F. Shchepetkin (2008a), Mesoscale to submesoscale transition in the California Current System: Part I. Flow structure, eddy flux and observational tests, *J. Phys. Oceanogr.*, *38*, 29–43, doi:10.1175/2007JPO3671.1.
- Capet, X., J. C. McWilliams, M. J. Molemaker, and A. F. Shchepetkin (2008b), Mesoscale to submesoscale transition in the California Current System. Part II: Frontal processes, *J. Phys. Oceanogr.*, *38*, 44, doi:10.1175/2007JPO3672.1.
- Capet, X., J. C. McWilliams, M. J. Molemaker, and A. F. Shchepetkin (2008c), Mesoscale to submesoscale transition in the California Current System. Part III: Energy balance and flux, *J. Phys. Oceanogr.*, *38*, 2256, doi:10.1175/2008JPO3810.1.
- Chelton, D. B., M. G. Schlax, M. H. Freilich, and R. F. Milliff (2004), Satellite measurements reveal persistent small-scale features in ocean winds, *Science*, *303*, 978–983, doi:10.1126/science.1091901.
- Chelton, D. B., M. G. Schlax, and R. M. Samelson (2007), Summertime coupling between sea surface temperature and wind stress in the California Current System, *J. Phys. Oceanogr.*, *37*, 495–517, doi:10.1175/JPO3025.1.
- Choboter, P. F., R. M. Samelson, and J. S. Allen (2005), A new solution of a nonlinear model of upwelling, *J. Phys. Oceanogr.*, *35*, 532–544.
- Choboter, P. F., D. Duke, J. P. Horton, and P. Sinz (2011), Exact solutions of wind-driven coastal upwelling and downwelling over sloping topography, *J. Phys. Oceanogr.*, *41*, 1277–1296.
- Debreu, L., P. Marchesiello, P. Penven, and G. Cambon (2012), Two-way nesting in split-explicit ocean models: Algorithms, implementation and validation, *Ocean Model.*, *49–50*, 1–21.
- Dekens, P. S., A. C. Ravelo, and M. D. McCarthy (2007), Warm upwelling regions in the Pliocene warm period, *Paleoceanography*, *22*, PA3211, doi:10.1029/2006PA001394.
- Dowsett, H. J., M. M. Robinson, and K. M. Foley (2009), Pliocene three-dimensional global ocean temperature reconstruction, *Clim. Past*, *5*, 769–783.
- Dowsett, H. J., et al. (2012), Assessing confidence in Pliocene sea surface temperatures to evaluate predictive models, *Nature Clim. Change*, *2*, 365–371, doi:10.1038/NCLIMATE1455.
- Edwards, K. A., A. M. Rogerson, C. D. Winant, and D. P. Rogers (2001), Adjustment of the marine atmospheric boundary layer to a coastal cape, *J. Atmos. Sci.*, *58*, 1511–1528.
- Enriquez, A. G., and C. A. Friehe (1995), Effects of wind stress and wind stress curl variability on coastal upwelling, *J. Phys. Oceanogr.*, *25*, 1651–1671.
- Etourneau, J., P. Martinez, T. Blanz, and R. Schneider (2009), Pliocene-Pleistocene variability of upwelling activity, productivity and nutrient cycling in the Benguela region, *Geology*, *37*, 871–874.
- Fedorov, A. V., C. M. Brierley, and K. Emanuel (2010), Tropical cyclones and permanent El Niño in the Pliocene epoch, *Nature*, *463*, 1066–1070, doi:10.1038/nature08831.
- Fedorov, A. V., C. M. Brierley, K. T. Lawrence, Z. Liu, P. S. Dekens, and A. C. Ravelo (2013), Patterns and mechanisms of early Pliocene warmth, *Nature*, *496*, 43–49, doi:10.1038/nature12003.
- Ford, H. L., A. C. Ravelo, P. S. Dekens, J. P. LaRiviere, and M. W. Wara (2015), The evolution of the equatorial thermocline and the early Pliocene El Padre mean state, *Geophys. Res. Lett.*, *42*, 4878–4887, doi:10.1002/2015GL064215.
- Fox-Kemper, B., and R. Ferrari (2008), Parameterization of mixed layer eddies. Part II: Prognosis and impact, *J. Phys. Oceanogr.*, *38*, 1166–1179, doi:10.1175/2007JPO3788.1.
- Fox-Kemper, B., R. Ferrari, and R. Hallberg (2008), Parameterization of mixed layer eddies. Part I: Theory and diagnosis, *J. Phys. Oceanogr.*, *38*, 1145–1165, doi:10.1175/2007JPO2792.1.
- Gill, A. E. (1982), *Atmosphere-Ocean Dynamics*, Academic Press, San Diego, Calif.
- Haney, R. L. (1971), Surface thermal boundary condition for ocean circulation models, *J. Phys. Oceanogr.*, *1*(4), 241–248.
- Haywood, A. M., P. J. Valdes, and V. L. Peck (2007), A permanent El Niño-like state during the Pliocene?, *Paleoceanography*, *22*, PA1213, doi:10.1029/2006PA001323.
- Haywood, A. M., et al. (2013), Large-scale features of Pliocene climate: Results from the Pliocene Model Intercomparison Project, *Clim. Past*, *9*, 191–209, doi:10.5194/cp-9-191-2013.
- Herbert, T. D., and J. Schuffert (1998), Alkenone unsaturation estimates of late Miocene through late Pliocene sea surface temperature changes, ODP Site 958, Proceedings of the Ocean Drilling Program, Scientific Results, 159T, 17–22, J. V. Firth, Ocean Drilling Program, College Station, Tex.
- Hurlburt, H. E., and J. D. Thompson (1973), Coastal upwelling on a β -plane, *J. Phys. Oceanogr.*, *3*, 16–32.
- Large, W. G., and S. Pond (1982), Sensible and latent heat flux measurements over the ocean, *J. Phys. Oceanogr.*, *12*, 464–482.
- Large, W. G., J. C. McWilliams, and S. C. Doney (1994), Oceanic vertical mixing: A review and a model with a nonlocal boundary layer parameterization, *Rev. Geophys.*, *32*, 363–403, doi:10.1029/94RG01872.
- LaRiviere, J. P., A. C. Ravelo, A. Crimmins, P. S. Dekens, H. L. Ford, M. Lyle, and M. W. Wara (2012), Late Miocene decoupling of oceanic warmth and atmospheric carbon dioxide forcing, *Nature*, *486*, 97–100, doi:10.1038/nature11200.
- Lentz, S. J., and D. C. Chapman (2004), The importance of nonlinear cross-shelf momentum flux during wind-driven coastal upwelling, *J. Phys. Oceanogr.*, *34*, 2444–2457.
- Locarnini, R. A., et al. (2013), *World Ocean Atlas 2013, Volume 1: Temperature*, vol. 73, NOAA Atlas NESDIS National Oceanic and Atmospheric Administration, Silver Spring, Md.
- Lynn, R. J., and S. J. Bograd (2002), Dynamic evolution of the 1997–1999 El Niño-La Niña cycle in the Southern California Current System, *Prog. Oceanogr.*, *54*, 59–75.
- Marchesiello, P., and P. Estrade (2009), Eddy activity and mixing in upwelling systems: A comparative study of Northwest Africa and California regions, *Int. J. Earth Sci.*, *98*, 299–308, doi:10.1007/s00531-007-0235-6.
- Marchesiello, P., and P. Estrade (2010), Upwelling limitation by onshore geostrophic flow, *J. Mar. Res.*, *68*, 37–62.
- Marchesiello, P., J. C. McWilliams, and A. Shchepetkin (2003), Equilibrium structure and dynamics of the California Current System, *J. Phys. Oceanogr.*, *33*, 753–783.
- Marchesiello, P., L. Debreu, and X. Covelard (2009), Spurious diapycnal mixing in terrain-following coordinate models: The problem and a solution, *Ocean Model.*, *26*, 156–169, doi:10.1016/j.ocemod.2008.09.004.
- Marlow, J. R., C. B. Lange, G. Wefer, and A. Rosell-Mele (2000), Upwelling intensification as part of the Pliocene-Pleistocene climate transition, *Science*, *290*, 2288–2291, doi:10.1126/science.290.5500.2288.
- McGregor, H. V., M. Dima, H. W. Fischer, and S. Mülitz (2007), Rapid 20th-century increase in coastal upwelling off Northwest Africa, *Science*, *315*, 637–639, doi:10.1126/science.1134839.

- Molnar, P., and M. A. Cane (2007), Early Pliocene (pre-Ice Age) El Niño-like global climate: Which El Niño?, *Geosphere*, 3(5), 337–365, doi:10.1130/GES00103.1.
- O'Brien, J. J., and H. E. Hurlburt (1973), A numerical model of coastal upwelling, *J. Phys. Oceanogr.*, 2, 14–26.
- Pedlosky, J. (1978a), An inertial model of steady coastal upwelling, *J. Phys. Oceanogr.*, 8, 171–177.
- Pedlosky, J. (1978b), A nonlinear model of the onset of upwelling, *J. Phys. Oceanogr.*, 8, 178–187.
- Penven, P., L. Debret, P. Marchesiello, and J. C. McWilliams (2006), Evaluation and application of the ROMS 1-way embedding procedure to the Central California Upwelling System, *Ocean Model.*, 12, 157–187.
- Philander, S. G., and A. Fedorov (2003), Role of tropics in changing the response to Milankovich forcing some three million years ago, *Paleoceanography*, 18, 1045, doi:10.1029/2002PA000837.
- Pickett, M. H., and J. D. Paduan (2003), Ekman transport and pumping in the California Current based on the U.S. Navy's high-resolution atmospheric model (COAMPS), *J. Geophys. Res.*, 108(C10), 3327, doi:10.1029/2003JC001902.
- Ravelo, A. C., K. T. Lawrence, A. Fedorov, and H. L. Ford (2014), A comment on "A 12-million-year temperature history of the tropical Pacific Ocean", *Science*, 346(6216), 1467.
- Renault, L., B. Dewitte, P. Marchesiello, S. Illig, V. Echevin, G. Cambon, M. Ramos, O. Astudillo, P. Minnis, and J. K. Ayers (2012), Upwelling response to atmospheric coastal jets off central Chile: A modeling study of the October 2000 event, *J. Geophys. Res.*, 117, C02030, doi:10.1029/2011JC007446.
- Samelson, R. M., and R. A. de Szoeke (1988), Semigeostrophic wind-driven thermocline upwelling at a coastal boundary, *J. Phys. Oceanogr.*, 18, 1372–1383.
- Schwing, F. B., T. Murphree, L. deWitt, and P. M. Green (2002), The evolution of oceanic and atmospheric anomalies in the northeast Pacific during the El Niño and La Niña events of 1995–2001, *Prog. Oceanogr.*, 54, 459–491.
- Scroton, N., S. G. Bonham, R. E. M. Rickaby, S. H. F. Lawrence, M. Hermoso, and A. M. Haywood (2011), Persistent El Niño–Southern Oscillation variation during the Pliocene Epoch, *Paleoceanography*, 26, PA2215, doi:10.1029/2010PA002097.
- Shchepetkin, A. F., and J. C. McWilliams (2003), A method for computing horizontal pressure-gradient force in an ocean model with a non-aligned vertical coordinate, *J. Geophys. Res.*, 108, 3090, doi:10.1029/2001JC001047.
- Shchepetkin, A. F., and J. C. McWilliams (2005), The Regional Oceanic Modeling System (ROMS): A split-explicit, free-surface, topography-following-coordinate oceanic model, *Ocean Model.*, 9, 147–404.
- Small, R. J., E. Curchitser, K. Hedstrom, B. Kauffman, and W. G. Large (2015), The Benguela upwelling system: Quantifying the sensitivity to resolution and coastal wind representation in a global climate model, *J. Clim.*, 28, 9409–9432, doi:10.1175/JCLI-D-15-0192.1.
- Spall, M. A., and N. Schneider (2016), Coupled ocean/atmosphere offshore decay scale of cold SST signals along upwelling eastern boundaries, *J. Clim.*, 29, 8317–8331, doi:10.1175/JCLI-D-16-0109.1.
- Steph, S., R. Tiedemann, M. Prange, J. Groeneveld, M. Schulz, A. Timmermann, D. Nürnberg, C. Rühlemann, C. Saukel, and G. H. Haug (2010), Early Pliocene increase in thermohaline overturning: A precondition for the development of the modern equatorial Pacific cold tongue, *Paleoceanography*, 25, PA2202, doi:10.1029/2008PA001645.
- Trenberth, K. E., W. G. Large, and J. G. Olson (1989), The effective drag coefficient for evaluating wind stress over the oceans, *J. Clim.*, 2, 1507–1516.
- Wara, M. W., A. C. Ravelo, and M. L. Delaney (2005), Permanent El Niño-like conditions during the Pliocene warm period, *Science*, 309, 758–761.
- Zaba, K. D., and D. L. Rudnick (2016), The 2014–2015 warming anomaly in the Southern California Current System observed by underwater gliders, *Geophys. Res. Lett.*, 43, 1241–1248, doi:10.1002/2015GL067550.